Development of Metal Inspection System Exploiting Magnetoresistive Sensors

Ibrahim Elshafiey and Ashraf Mohra

Abstract— Advances in magnetoresistive (MR) type sensors provide a new technique for nondestructive evaluation NDE of metal structures. MR sensors include high sensitivity and reduced size. Being produced by thin film processing techniques, the manufacturing cost of these sensors is low. This paper provides an attempt to develop an NDE system that depends on one type of MR sensors, namely the giant MR (GMR) elements. An example is considered of detecting defects in printed circuit boards. System details and experimental results are provided. Computational modeling validation is introduced based on finite element analysis.

I. Introduction

Nondestructive evaluation (NDE) is essential for ensuring the integrity of various engineering systems. Examples of such systems include power plants, natural gas and oil industry, pressure vessels and aircraft. Evaluation of such systems starts during the manufacturing process and continues along their life span to detect the initiation of defects in metallic parts due to corrosion or fatigue cracks. Conventional inspection techniques, such as eddy-current inspection using coil magnetometers, x-radiography, ultrasonic, and acoustic emission suffer from limitations in key areas such as: difficulty in locating hidden subsurface defects, use of bulky or hazardous equipment, insufficient spatial resolution, slow speed of inspection, high cost of equipment, and complexity of analyzing the data output by such systems.

This paper proposes the use of sensitive magnetoresistive (MR) sensors in imaging the magnetic field maps. MR sensors have been used for advanced applications including high density of 50 Gb/in^2 magnetic recording, Everitt, et al. [1]. MR sensors have also been suggested for use in nondestructive evaluation as in the system introduced by Rempt, from Boeing company using an array of eight sensors in examining aircraft [1]. A GMR based rotating probe system is introduced in NASA Langley Research Center, as explained by Wincheski, et al. [2].

The paper focuses on a new NDE application using MR sensors related to printed circuit board PCB inspection. Details about MR sensors are introduced next followed by inspection problem formulation, simulation as well as experimental results.

Proceedings of The 6th IEEE International Workshop on System-on-Chip for Real-Time Applications, December 27 - 29, 2006, Cairo, Egypt

This work was supported by SABIC Company, under research grant number 27/426.

I. Elshafiey is with the Electrical Engineering Department, King Saud University, Riyadh, 11421, SA. (phone: 966-50-9338004, fax: 966-1-4676757, email: ishafiey@ksu.edu.sa).

A. Mohra is with the Electrical Engineering Department, King Saud University, Riyadh, 11421, SA. (email: amohra@ksu.edu.sa).

II. Magnetoresistance Sensors

Magnetoresistive sensor technologies offer significant advantages in NDE systems. A key advantage of MR sensors is in flat frequency response extending from dc to few MHz [4], making them particularly attractive for low-frequency and multi-frequency detection for deep-flaw detection and depth profiling. The reduced size of these sensors helps detect small and deep flaws which are usually one order of magnitude smaller than surrounding features of the object. MR sensors are mass produced by thin film processing techniques similar to integrated circuit manufacturing, Jander et al. [5], and thus fabrication process is compatible with silicon circuit technology, allowing integration of sensors with on-chip signal processing. MR sensors can easily be produced in dense arrays for rapid, single-pass scanning of large areas. The low power consumption of MR sensors enables the assembly of compact sensor arrays on a variety of substrates. Arrays have been fabricated with sensor spacing as small as 5 μm [5].

One type of MR sensors is the high sensitivity giant magnetoresistive (GMR) element. Large magnetic field dependent changes are possible in thin-film ferromagnetic/non-magnetic multilayers [6]. The GMR phenomenon was first observed in France in 1988 [7]. The principle of GMR is to obtain a change in resistance for thin ferromagnetic layers encapsulating a nonmagnetic layer according to the direction of magnetic moments. If the two ferromagnetic layers possess parallel magnetization moments, there will be less scattering for electrons at the interface. There will be thus longer free path and less resistance. The opposite is true if the magnetic moments in the ferromagnetic layers are antiparallel. GMR sensors provide a 98% linear output from 10% to 70% of full scale, a large magnetoresistive effect (13% to 16%), a stable temperature coefficient (0.14% per °C), temperature tolerance (150 °C), and a large magnetic field range (0 to 300) Gauss as illustrated in [8].

1-4244-0898-9/06/$20.00 ©2006 IEEE.

Authorized licensed use limited to: KING SAUD UNIVERSITY. Downloaded on May 17, 2009 at 08:02 from IEEE Xplore. Restrictions apply.

III. PCB INSPECTION

PCB inspection has been suggested using eddy-current testing probe [9]. Spin-valve giant magnetoresistance SV-GMR sensor has been shown to be successful in inspecting defects on both the top and bottom layer of high density double layer PCB [10]. This paper examines inspection of meander type coil such as the one used in high-frequency excitation for eddy current testing of microbeads [11].

Coil structure is shown in Fig. 1 with a defect in the metal. The inspection depends on injecting dc current in the metal part and testing the magnetic field with a GMR sensor. The sensor type suggested for use in the experimental setup is manufactured by NVE Corporation, part number AA003-02 with the following specifications: saturation field is 50 Oe, linear range 5-35 Oe, and die size is 411x1458 μm. The sensor is formed as a Wheatstone bridge of four resistors of 5 kΩ ± 20%. Two resistors are shielded from surrounding magnetic field while the others are exposed to obtain an output voltage proportional to applied field. The sensitivity of the sensor ranges from 2-3.2 mV/V-Oe. Am image of two sensors on top of Saudi coin is shown in Fig. 2.

The architecture of the sensor depends on a multilayer structure, where anti-ferromagnetic coupling occurs between two layers in multilayer structure. As a result these sensors are not affected by extremely large fields, at temperatures below 300°C, and will resume normal operation after the large field is removed.

To examine the sensor the magnetic field is recorded on varying distance from a wire carrying a dc current of 10A as shown in Fig. 3. Results present comparison of normalized magnitude magnetic flux density $\boldsymbol{B}$ versus distance from wire, compared to analytical field values given as

$$B = \mu_0 \frac{I}{2\pi\rho} \tag{1}$$

where μ_0 is the permeability of the free space determined as $4\pi x10^{-7}$ Henry/m, I is the current in A, and ρ is the normal distance from the wire in m.

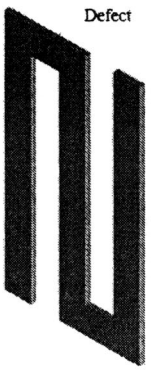

Fig. 1. 3D view of the metal part to be inspected.

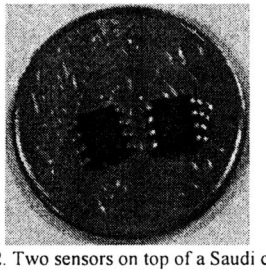

Fig. 2. Two sensors on top of a Saudi coin.

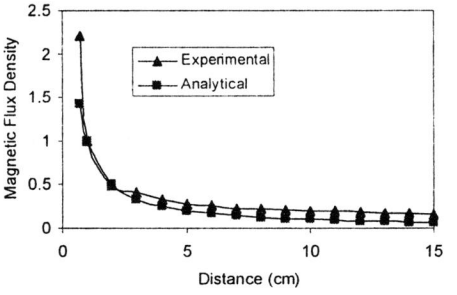

Fig. 3. Experimental validation of the GMR sensor.

IV. COMPUTATIONAL MODELING

Finite element analysis is invoked to model the configuration under test. In this formulation, for both static fields, the governing Maxwell's equations are

$$\nabla \times \boldsymbol{H} = \boldsymbol{J} \tag{2}$$

$$\nabla \cdot \boldsymbol{B} = 0 \tag{3}$$

Subject to the material constitutive relationship, $\boldsymbol{B} = \mu \boldsymbol{H}$, where $\boldsymbol{B}$, and $\boldsymbol{H}$, are the magnetic flux density and magnetic field intensity, respectively. $\boldsymbol{J}$ is the current density and μ is the permeability of material.

The solution is easily obtained by representing the fields in terms of potential functions such that

$$\boldsymbol{B} = \nabla \times \boldsymbol{A} \tag{4}$$

Potential representation of the field guarantees the satisfaction of (2) and (3), and the equations can be rewritten as:

$$\nabla \times (\nu \nabla \times \boldsymbol{A}) = \boldsymbol{J} \tag{5}$$

where the reluctivity ν is the inverse of the permeability μ. For linear isotropic materials and assuming Coulomb Gauge ($\nabla \cdot \boldsymbol{A} = 0$), Equation 3.5 reduces to [12]

$$-\nu \nabla^2 \boldsymbol{A} = \boldsymbol{J} \tag{6}$$

Commercial finite element analysis package Ansys, is used in the solution of the problem [13]. Details of model and results are given next.

Authorized licensed use limited to: KING SAUD UNIVERSITY. Downloaded on May 17, 2009 at 08:02 from IEEE Xplore. Restrictions apply.

V. Modeling Results

Three dimensional modeling is used to simulate this problem. Three element types are considered. Elements corresponding to air and crack have nodal degree of freedom consisting of the three components of the magnetic vector potential A. Elements corresponding to the meander coil have scalar potential V degree of freedom, in addition to the components Ax, Ay and Az. The third element type is used to deal with the infinite unbounded 3D nature of the problem. A single layer is used on the outer surface using semi-infinite elements with three degrees of freedom corresponding to A. Solenoidal formulation is adopted to automatically satisfy the solenoidal condition of zero divergence of current density. This type of formulation results in nonlinear analysis with symmetric global matrix.

Figure 4 shows a plan view of mesh of the meander coil on top of the dielectric substrate. The size of meander coil strip width is chosen to be 5 mm and the length is 5 cm. Total number of elements is 119202 among which 114075 elements are of first type, 2071 are of second type for source, and 3056 are for semi-infinite elements. Source excitation is done by applying current injection on the hot port of the coil, while the other port is grounded. The voltage degree of freedom is coupled on all nodes of the coil on the source injection side.

Figure 5 presents vector map of current density in the area of the defect. The figure shows how current rotates around the defect. Figure 6 (a-c) shows the changes in the x, y and z components of the magnetic flux density $\underline{B}$ due to the presence of defect. Two defect types are considered, with 1 mm and 1.5 mm width, respectively. Defect length is fixed at 3 mm, parallel to long arms of the coil.

VI. Experimental Results

Experimental testing was conducted on a meander type coil with various defects as shown small rectangles in Fig. 7. DC current was injected in the coil and magnetic field was detected to obtain A-scans. Figure 7 shows 4 lines upon which a scanning was done. Results in terms of sensor reading are shown in Fig. 8.

VII. Discussions

Magnetic field maps can be used to monitor the status of metal structures. The technique depends on exciting the specimen by a current and measuring the magnetic field components using magnetoresistive sensors. Giant magnetoresistive sensors have high sensitivity that allows detection of changes in magnetic flux density values, due to the presence of material flaws. Modeling results of the example considered in this paper of inspecting meander type

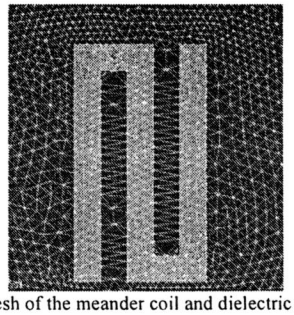

Fig. 4. Mesh of the meander coil and dielectric substrate.

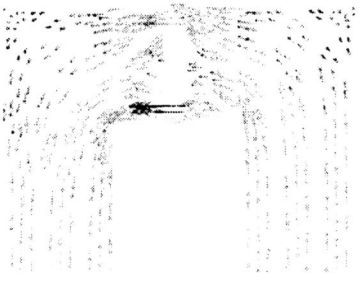

Fig. 5. Simulated current distribution arround the defect.

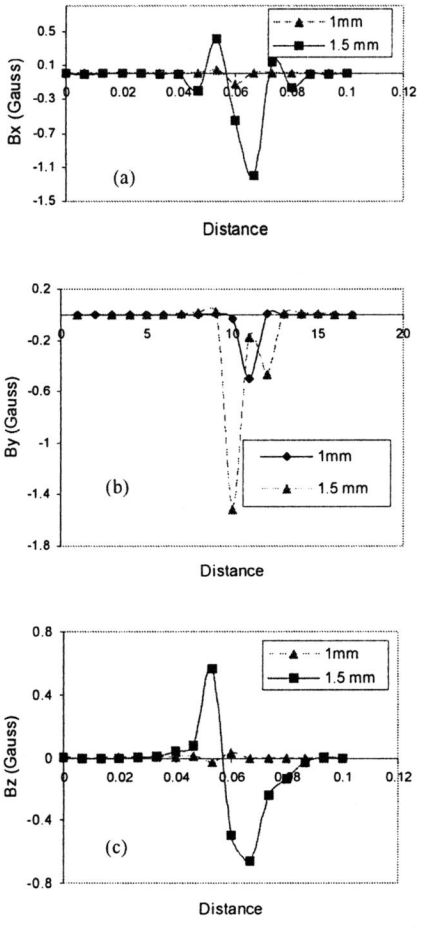

Fig. 6. Variation in the three components of magnetic flux density for parallel components Bx (a) and By (b) and normal component Bz (c). Two defect sizes (1 mm and 1.5 mm width) are considered

Authorized licensed use limited to: KING SAUD UNIVERSITY. Downloaded on May 17, 2009 at 08:02 from IEEE Xplore. Restrictions apply.

coil showed that there is a noticeable change in field values that could be detected with commercially available GMR sensors.

A setup was built to use the sensor in detecting metal flaws. The A-scans point to the locations of defects. The orientation and the magnetic hysteresis of GMR sensors were found to affect the reproducibility of the measurements and further investigation is required to tackle these challenges.

One key advantage of MR sensors is that they can be batch fabricated to obtain an array structure. Design of 20 GMR sensors with 0.5 mm pitch on a polyimide film was suggested by Kataoka at al. at Shinsu University [14]. Success in fabrication of GMR sensor arrays would have a considerable impact on enhancing the application of this technology in NDE.

REFERENCES

[1]. B. A. Everitt, D. Olson, T. v. Nguyen, N. Amin, T. Pokhil, P. Kolbo, L. Zhong, and Ed Murdock, "Vertical Giant Magnetoresistive Read Heads for 50-Gb/in^2 Magnetic Recording," *IEEE Trans. Magn.*, vol. 41, pp. 125-131, 2005.

[2]. R. Rempt, "Scanning with Magnetoresistive Sensor for Subsurface Corrosion," in *Review of Progress in QNDE*. vol. 21, D. O. Thompson and D. E. Chimenti, Eds., pp. 1771-1778, 2002.

[3]. B. Wincheski, J. Simpson, M. Namkung, et al., "Development of Giant Magnetoresistive Inspection System for Detection of Deep Fatigue Cracks under Airframe Fasteners," in *Review of Progress in QNDE*. vol. 21, D. O. Thompson and D. E. Chimenti, Eds., pp. 1007-1014, 2002.

[4]. T. Dogaru and S. T. Smith, "Integrated giant magnetoresistive transducer for eddy current testing," in *15th WCNDT* Roma, 2000.

[5]. A. Jander, C. Smith, and R. Schneider, "Magnetoresistive Sensors for Nondestructive Evaluation," in *the 10th SPIE Int. Symposium, Nondestructive Evaluation for Health Monitoring and Diagnostics*, 2005.

[6]. M. Caruso, T. Bratland, et al. "A New Perspective on Magnetic Field Sensing," Electronically available at www.ssec.honeywell.com, 1998.

[7]. M. Baibich, J. Broto, et al, "Giant Magnetoresistance of (001)Fe/(001)Cr Magnetic Superlattices," Phys. Rev. Lett., Vol. 61, 2472-2475, 1988.

[8]. "Introduction to NVE GMR Sensors," Electronic Data Sheet of NVE Sensors, www.nve.com.

[9]. S. Yamada, K. Chomsuwan, Y. Fukuda, M. Iwahara, H. Wakiwaka, and S. Shoji, "Eddy-Current Testing Probe With Spin-Valve Type GMR Sensor for Printed Circuit Board Inspection," *IEEE Trans. Magn.*, vol. 40, pp. 2676-2678, 2004.

[10]. K. Chomsuwan, S. Yamada, M. Iwahara, H. Wakiwaka, and S. Shoji, "Application of Eddy-Current Testing Technique for High-Density Double-Layer Printed Circuit Board Inspection," *IEEE Trans. Magn.*, vol. 41, pp. 3619-3621, 2005.

[11]. S. Yamada, K. Chomsuwan, T. Hagino, H. Tian, K. Minamide, and M. Iwahara, "Conductive Microbead Array Detection by High-Frequency Eddy-Current Testing Technique with SV-GMR Sensor," *IEEE Trans. Magn.*, vol. 41, pp. 3622-3624, 2005.

[12]. Meeker, D., *Finite Element Method Magnetics: User's Manual*, available online at http://femm.foster-miller.net, 2006.

[13]. Ansys Inc., www.ansys.com.

[14]. Y. Kataoka, S. Murayama, et al., "Application of GMR Line Sensor to detect the magnetic flux distribution for nondestructive testing," Int. J. Appl. Electromagn. Mech., Vol. 15, pp. 47, 2001.

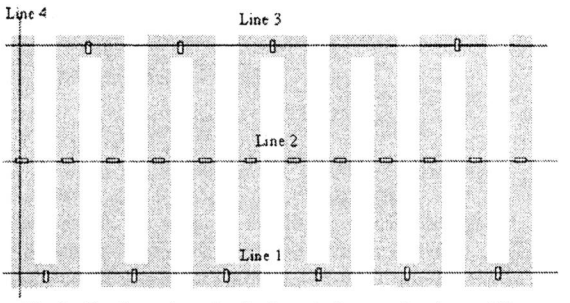

Fig. 7. Configuration of coil. Scan is done on the shown 4 lines.

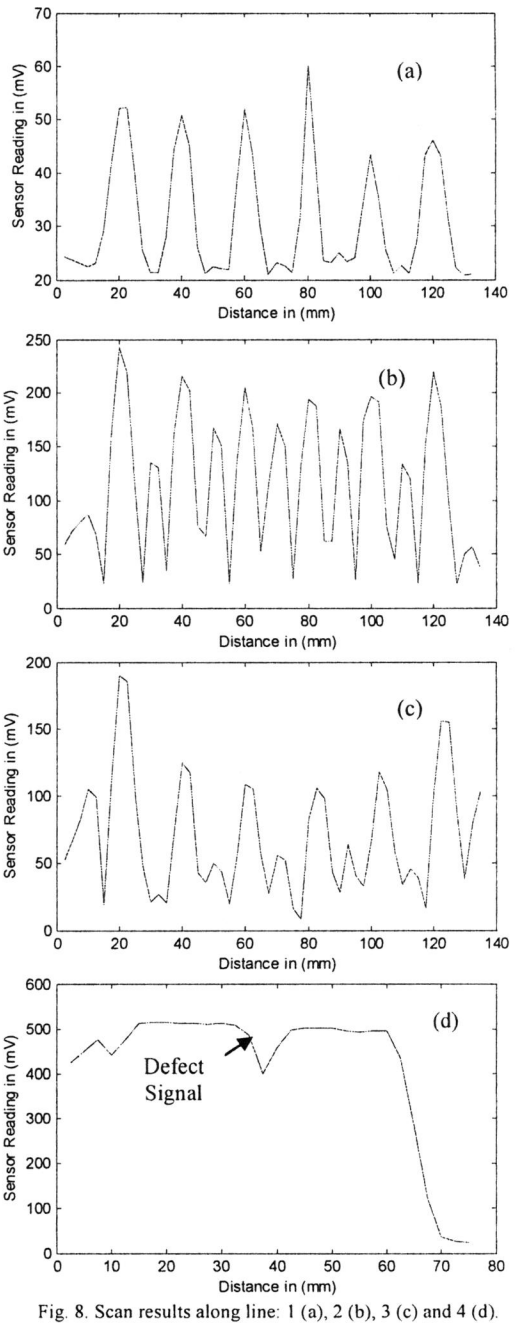

Fig. 8. Scan results along line: 1 (a), 2 (b), 3 (c) and 4 (d).

Authorized licensed use limited to: KING SAUD UNIVERSITY. Downloaded on May 17, 2009 at 08:02 from IEEE Xplore. Restrictions apply.